Case Studies in Thermal Engineering 49 (2023) 103280

Contents lists available at ScienceDirect

Case Studies in Thermal Engineering

journal homepage: www.elsevier.com/locate/csite

New fractional approach for *CMC* and water based hybrid nanofluid with slip boundary layer: Applications of fractal fractional derivative

Ali Raza [a,b], Rifaqat Ali [c], Sayed M. Eldin [d], Suleman H. Alfalqui [c], Ali Hasan Ali [e,f,g,*]

[a] Department of Mathematics, Minhaj University, Lahore, Pakistan
[b] Department of the Mathematics, University of Engineering and Technology, Lahore, Pakistan
[c] Department of Mathematics, College of Science and Arts, Muhayil, King Khalid University, Abha, Saudi Arabia
[d] Faculty of Engineering and Technology, Future University in Egypt, New Cairo, 11835, Egypt
[e] Institute of the Mathematics, University of Debrecen, Pf. 400, H-4002, Debrecen, Hungary
[f] Department of Mathematics, College of Education for Pure Sciences, University of Basrah, Basrah 61001, Iraq
[g] College of Engineering Technology, National University of Science and Technology, Dhi Qar 64001, Iraq

ARTICLE INFO

Keywords:
Brinkman type fluid
Sinusoidal conditions
Laplace transformation
Slip effects
Fractal fractional derivatives

ABSTRACT

The physical significance of the Fractal fractional derivative, one of the most fascinating and modern analytical techniques, to the thermal flow is described in this paper. Free convection, which is the flow of an erratic, incompressible viscous fluid on a vertically inclined plate, has been considered in this work. Two types of base fluids, namely water and carboxymethyl cellulose, are used in the presence of graphene oxide (GO) and molybdenum disulfide (MoS_2) nanoparticles. The flow is subject to slip possessions due to the inclined surface. The non-dimensional leading equations for thermal and momentum, under Boussinseq's approximation, can be solved by employing a Laplace transformation scheme, the fractal fractional derivative, and a more recent and improved definition of a fractional mathematical term. The thermal expressions are modeled using the Laplace transformation. The effect and comparison of various parameters are then visually and quantitatively analyzed after this activity. We, therefore, proposed that a water-based nanofluid's thermal profile and velocity are marginally higher than those of a hybrid nanofluid based on carboxymethyl cellulose. The momentum profile additionally illustrates the dual behavior of the flowing hybrid nanofluid as the fluid parameter of the Brinkman type increases.

1. Introduction

In recent decades, many industrial and scientific fields, including electronics and power generation, where heat transfer is frequent, have seen fast growth in nanotechnology. Specialized heat transfer management is necessary due to the added technological advancement. Numerous researchers have attempted to study an effective heat transmission medium. Many techniques, like the microchannel and increasing surface area, have been tried but failed because of scientific limitations. To increase heat transfer rates, several nanofluids have been defined and researched. Nanofluids are made by mixing nanoparticles with conventional base fluids [1].

* Corresponding author. Institute of the Mathematics, University of Debrecen, Pf. 400, H-4002, Debrecen, Hungary.
E-mail addresses: aliraza.math@mul.edu.pk (A. Raza), rrafat@kku.edu.sa (R. Ali), elsayed.tageldin@fue.edu.eg (S.M. Eldin), salfalqui@kku.edu.sa (S.H. Alfalqui), ali.hasan@science.unideb.hu (A.H. Ali).

https://doi.org/10.1016/j.csite.2023.103280
Received 4 April 2023; Received in revised form 24 June 2023; Accepted 9 July 2023
Available online 10 July 2023

The fundamental fluids contain nanoparticles of different types. Since the beginning, scientists have worked to find a solution to this issue to enhance the properties of diverse fluid types. They are working to fix the flaws in these common fluids. Choi and Eastman initially discovered the nanoparticle dispersion in the base fluid. Several researchers have defined, created, and tested many Nanofluids in heat transfer applications [2]. The interaction of nanoparticles with base fluids has been the subject of numerous theoretical and experimental studies. In primary fluids like oil, water, and concrete, nanoparticles like carbon in various forms, carbide ceramics, nitride ceramics, and metallic oxides are frequently utilized.

Over the past few decades, a great deal of theoretical and numerical research has been done on the rheological and thermal transfer properties of hybrid/traditional nanofluid flow. Gyrotactic microorganisms were investigated mathematically by Bhatti et al. [3] on a stretching plate. Between vertical parallel plates, a nanofluid transient free convection radiative flow was studied by Hajizadeh et al. [4]. The impact of nanoparticles on slip blood flows in arterial arteries was later discovered by Seikh et al. [5]. Ibrahim and Kuma [6] looked at the high-order slip flow that results from a curved stretchable surface. The symmetric nanofluid movement at a curved surface was studied by Khan et al. [7]. According to Nadeem et al. [8], a viscous nanofluid near the stagnation point may flow toward the circular cylinder with mass suction. In their analysis of the hybrid base nanofluid, Gholinia et al. [9] take the porous stretchable cylinder into account. Dusty hybrid nanofluid with slippage and radiative flow, hybrid nanofluid, is more effective at transporting heat than standard nanofluid, claim Souayeh et al. [10]. Moreover, Waini & Nadeem et al. [11,12] developed boundary layer flow studies that employed hybrid nanofluid at the circular cylinder. In the study article that follows [13–18], several fresh numerical investigations relating to diverse hybrid nanofluid flow challenges are offered.

The modern research community has effectively applied certain novel fractional derivative concepts to examine many kinds of mathematical models. The essential fluids and heat or mass transmission models are given precedence among them. The fractal-fractional derivative has recently been proposed, although it is not employed for heat transfer in channel flow [19–22]. The goal of fractional calculus is to expand classical calculus to include derivatives of non-integer order. Due to the use of ordinary and partial differential equations with a semi-order of differentiation, modeling the viscous behavior of fluid materials has significantly improved in recent years. Over the past ten years, several generalized fractional derivatives, such as the Caputo, Caputo-Fabrizio, and constant proportional Caputo derivatives, have been published in the scientific literature. The non-integer order derivative can be used to describe a wide range of physical events [23–27].

To solve the challenges in practical situations, Atangana has looked at the relationships between fractal and fractional derivatives [28]. Atangana et al. [29,30] also thoroughly assessed freshly created operators to solve fractal finite difference equations the year before. Imran recently looked at the fractal fractional derivative to determine how viscous fluid flows. MHD modifies the flow between two parallel plates that are indefinitely stretched. Unfortunately, the novel fractal-fractional derivative idea has not been applied to study the fluid flow heat transfer problem yet. A branch of mathematics known as fractional calculus was created expressly to express many engineering phenomena, including fluid and nanofluid dynamics, thermal science, and other related fields. They emphasized relaxation compliance and creep modulus using fractal Maxwell and Kelvin models and suggested that local fractal differential operators might aid in memory storage and reduce processing costs. The existence and uniqueness of the positive solution to the heat flow equation were proven by using fractional-fractal differentiation. Also, work on fractional calculus may continue, but we'll wrap up a few current projects involving fractal-fractional differential operators [31] and fractional differential operators [32]. Our suggestion that the Newtonian fluid (ordinary liquid) is magnetised by dispersion into porous media was influenced by the works on fractal-fractional and just fractional differential operators cited above. We use fractal-fractional derivatives of the power law to build a mathematical model of ferromagnetic fluid. The MHD Newtonian fluid model is fractal-fractionalized and embedded in a porous substance using a power law kernel. This is accomplished by using a powerful Laplace transform strategy. Our research is the initial

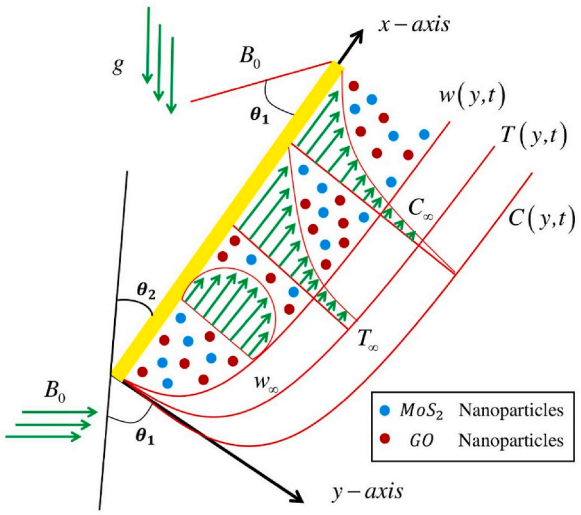

Fig. 1. Geometry of the flow problem.

application of the ground-breaking fractal-fractional derivative approach to a heat transfer issue.

Based on the literature mentioned earlier, this work considers free convection, unsteady, and incompressible viscous fluid on a vertically inclined plate. Graphene oxide (*GO*) and molybdenum disulfide (MoS_2) nanoparticles are employed in the presence of two different base fluids, specifically water and carboxymethyl cellulose. The non-dimensional model equation for momentum and energy is used, together with a more recent and improved definition of a fractional mathematical term, the fractal fractional derivative, and a Laplace transformation scheme. Moreover, a more modern definition of fractional derivative, namely Fractal fractional derivative, is used to examine the effects of various hybrid nanofluids and limitations.

2. Problem description

Suppose an unsteady, viscous, incompressible Brinkman-type hybrid-nanofluid flows on an infinite inclined plate. The inclined magnetic field also considers sinusoidal heat and slip boundary conditions. Initially at $t = 0$, the plate and fluid both are at rest position with the constant temperature at T_∞. Then with the passage of time at $t = 0^+$, the inclined poured plate starts to vibrate with some constant velocity $U_o H(t) Cos(\omega t)$, where ω symbolize the amplitude of the motion, and fluid starts to flow on the vertical plate. The suspension of different hybrid nanofluids moves with the same velocity as the velocity of poured plate. Due to shear, the fluid is constantly moving with velocity components of $w(y,t)$. Fig. 1 is depicted for the flow analysis.

By considering these conditions and with the help of Boussinseq's approximation, the leading equations for fluid and thermal transport can be mathematically defined as [21].

$$\rho_{nf}\left(\frac{\partial w(y,t)}{\partial t}+\beta_1^*w(y,t)\right)=\mu_{nf}\frac{\partial^2 w(y,t)}{\partial y^2}-\left(\sigma_{nf}B_o^2\,sin(\theta_1)+\frac{\mu_{nf}\varphi}{K}\right)w(y,t)+g(\rho\beta_T)_{nf}(T(y,t)-T_\infty)cos(\theta_2)$$
$$+g(\rho\beta_c)_{nf}(C(y,t)-C_\infty)cos(\theta_2) \tag{1}$$

$$\left(\rho C_p\right)_{nf}\frac{\partial T(y,t)}{\partial t}=k_{nf}\frac{\partial^2 T(y,t)}{\partial y^2} \tag{2}$$

$$\frac{\partial C(y,t)}{\partial t}=D\frac{\partial^2 C(y,t)}{\partial y^2} \tag{3}$$

With correspondent conditions:

$$w_{(y,0)}=0, T_{(y,0)}=T_\infty, C_{(y,0)}=C_\infty;\quad t=0$$

$$w_{(0,t)}-h\left.\frac{\partial w}{\partial y}\right|_{y=0}=U_oH(t)Cos(\omega t), C_{(0,t)}=C_w$$

$$T_{(0,t)}=\begin{cases}T_\infty+\left(T_{(y,t)}-T_\infty\right)\dfrac{t}{t_o}, 0\le t\le t_o\\ T_w, t>t_o\end{cases}$$

$$w_{(y,t)}\to 0, T_{(y,t)}\to T_\infty, C_{(y,t)}\to C_\infty\quad ;\quad y\to\infty, t>0$$

Include the following non-dimensional constants to non-dimensionalize the preceding equations and associated conditions.

$$w^*=\frac{w}{U_o}, y^*=\frac{U_o}{\upsilon_f}y, t^*=\frac{U_o^2}{\upsilon_f}t, T^*=\frac{T_{(y,t)}-T_\infty}{T_w-T_\infty}, C^*=\frac{C_{(y,t)}-C_\infty}{C_w-C_\infty}$$

$$Pr=\left(\frac{\mu C_p}{\kappa}\right)_f, Gr=\frac{g(\rho\beta_T)_f(T_w-T_\infty)}{U_o^3}, Gm=\frac{g(\rho\beta_c)_f\Delta C_{(y,t)}}{U_o^3}, \beta_1^*=\frac{\upsilon_f}{U_o^2}\beta_2$$

We get the following dimensionless equations by substituting the above constraints into the leading equations (1)–(3) without using the staric notation.

$$\Pi_o\frac{\partial w_{(y,t)}}{\partial t}=\Pi_1\frac{\partial^2 w_{(y,t)}}{\partial y^2}-\beta_2 w_{(y,t)}-\left(\Pi_2 Msin(\theta_1)+\frac{\Pi_1}{K}\right)w(y,t)+\Pi_3 GrT_{(y,t)}\,cos(\theta_2)+\Pi_4 GmC_{(y,t)}\,cos(\theta_2) \tag{4}$$

$$\Pi_5\,Pr\frac{\partial T_{(y,t)}}{\partial t}=\frac{\partial^2 T_{(y,t)}}{\partial y^2} \tag{5}$$

$$Sc\frac{\partial C_{(y,t)}}{\partial t}=\frac{\partial^2 C_{(y,t)}}{\partial y^2} \tag{6}$$

Along with dimensionless conditions:

$$w_{(y,0)} = 0, T_{(y,0)} = 0, C_{(y,0)} = 0 \quad ; \quad t = 0 \tag{7}$$

$$w_{(0,t)} - h\left.\frac{\partial w}{\partial y}\right|_{y=0} = H(t)Cos(\omega t), T_{(0,t)} = \begin{cases} t, 0 \le t \le 1 \\ \\ 1, t > 1 \end{cases}, C_{(0,t)} = 1 \tag{8}$$

$$w_{(y,t)} \to 0, T_{(y,t)} \to 0, C_{(y,t)} \to 0 \quad ; \quad y \to \infty, t > 0 \tag{9}$$

In the above conditions (7–9), condition (7) is an initial condition at $t = 0$ where the whole system is at rest condition, and condition (8) is a boundary condition at $y = 0$ where the velocity and temperature fields will vary accordingly with constant concentration. At the same time, the last condition (9) is also a boundary condition at $y \to \infty$ where the whole governed model is again consistent. Tables 1 and 2 provide the various thermal properties of the discussed fluids and nanoparticles.

where:

$$\Pi_o = \left(1 - \varphi_{nf}\right) + \frac{\varphi\rho_s}{\rho_s}, \Pi_1 = \frac{\mu_f}{(1-\varphi)^{2.5}}$$

$$\Pi_2 = 1 + \frac{3\left(\frac{\sigma_s}{\sigma_f} - 1\right)\varphi}{\left(\frac{\sigma_s}{\sigma_f} + 2\right) - \left(\frac{\sigma_s}{\sigma_f} - 1\right)\varphi}, \Pi_3 = (1-\varphi) + \frac{\varphi(\rho\beta_T)_s}{(\rho\beta_T)_f}$$

$$\Pi_4 = (1-\varphi) + \frac{\varphi\left(\rho C_p\right)_s}{\left(\rho C_p\right)_f}, \Pi_5 = \frac{k_{nf}}{k_f}$$

3. Basic definitions

The fractional derivative of y of order (β) in the RL-form with power, the law can be written as follows, considering that $y(x)$ is a continuous function.

$$^{FFP}\mathfrak{D}_x^{\alpha,\beta} y(x) = \frac{1}{\Gamma(1-\alpha)} \frac{d}{dx^\beta} \int_0^x y(t)(x-t)^{-\alpha} dt, 0 < \alpha, \beta \le 1$$

$$\frac{dy(t)}{dx^\beta} = \lim_{x \to t} \frac{y(x) - y(t)}{x^\beta - t^\beta} \tag{10}$$

Usual Laplace Transformation: Consider defining $y(x)$ in the case where $(x > 0)$. The Laplace integral provides a non-fractional transform known as the LT of $y(x)$, which is clearly defined as $Y(s)$ or $\mathscr{L}\{y(x)\}$.

$$\mathscr{L}\{y(x)\} = Y(x) = \int_0^\infty exp(-sx) f(x) dx \tag{11}$$

Fractal Laplace Transformation: If $g(x)$ is a continuous function, then [12] is a description of its fractal-Laplace

$$^{F}\mathscr{L}_p^\alpha\{g(x)\} = G(x) = \int_0^\infty exp(-sx) x^{\alpha-1} g(x) dx \tag{12}$$

And for $\alpha \to 1$ the usual Laplace can be attained.

Table 1
Lists of the flexibility for considered hybrid nanofluids.

Quantities	Nanofluid	Hybrid Nanofluid
Density	$\rho_{nf} = (1-\varphi)\rho_f + \varphi\rho_s$	$\rho_{hnf} = (1-\varphi_{hnf})\rho_f + \varphi_{GO}\rho_{GO} + \varphi_{MoS_2}\rho_{MoS_2}$
Dynamic Viscosity	$\mu_{nf} = \mu_f/(1-\varphi)^{5/2}$	$\mu_{hnf} = \mu_f/[1-(\varphi_{MoS_2} + \varphi_{GO})]^{5/2}$
Electrical conductivity	$\sigma_{nf}/\sigma_f = 1 + 3(\sigma_s/\sigma_f - 1)\varphi/(\sigma_s/\sigma_f + 2) - (\sigma_s/\sigma_f - 1)\varphi$	$\sigma_{hnf}/\sigma_f = 1 + 3(\varphi_{MoS_2}\sigma_{MoS_2} + \varphi_{GO}\sigma_{GO}/\sigma_f - \varphi_{hnf})/\varphi_{MoS_2}\sigma_{MoS_2} + \varphi_{GO}\sigma_{GO}/\varphi_{hnf}\sigma_f + 2 - (\varphi_{MoS_2}\sigma_{MoS_2} + \varphi_{GO}\sigma_{GO}/\sigma_f - \varphi_{hnf})$
Thermal conductivity	$K_{nf}/K_f = k_s + 2k_f - 2\varphi(k_s - k_f)/k_s + 2k_f + \varphi(k_s - k_f)$	$K_{hnf}/K_f = \varphi_{MoS_2}k_{MoS_2} + \varphi_{GO}k_{GO}/ - \varphi_{hnf} + 2k_f + 2(\varphi_{MoS_2}k_{MoS_2} + \varphi_{GO}k_{GO}) - 2\varphi_{hnf}K_f/\varphi_{MoS_2}k_{MoS_2} + \varphi_{GO}k_{GO}/\varphi_{hnf} + 2k_f + (\varphi_{MoS_2}k_{MoS_2} + \varphi_{GO}k_{GO}) - \varphi_{hnf}K_f$
Heat capacitance	$(\rho C_p)_{nf} = (1-\varphi)(\rho C_p)_f + \varphi(\rho C_p)_s$	$(\rho C_p)_{hnf} = (1-\varphi_{hnf})(\rho C_p)_f + \varphi_{MoS_2}(\rho C_p)_{MoS_2} + \varphi_{GO}(\rho C_p)_{GO}$
Thermal Expansion Coefficient	$(\rho B_T)_{nf} = (1-\varphi)(\rho B_T)_f + \varphi(\rho B_T)_s$	$(\rho B_T)_{hnf} = (1-\varphi_{hnf})(\rho B_T)_f + \varphi_{MoS_2}(\rho B_T)_{MoS_2} + \varphi_{GO}(\rho B_T)_{GO}$

Table 2
The thermal characteristics of nanoparticles.

Material	Water	*CMC*	MOS_2	*GO*
$\rho(kg/m^3)$	997.1	997	5060	1800
$C_p(J/kg\,K)$	4179	4179	397.21	717
$k(W/m\,K)$	0.613	0.613	904.4	5000
$\beta_T(K^{-1})$	21	70×10^{-5}	2.842×10^{-5}	2.84×10^{-4}

4. Governed fractal fractional model

It is possible to use the Fractal fractional model for the guided problem as

$$ {}^{C}\mathfrak{D}_t^{\alpha}\,\Pi_o w_{(y,t)} = \beta t^{\beta-1}\left\{\Pi_1\frac{\partial^2 w_{(y,t)}}{\partial y^2} - \beta_2 w_{(y,t)} - \left(\Pi_2 Msin(\theta_1) + \frac{\Pi_1}{K}\right)w(y,t) + \Pi_3 GrT_{(y,t)}\,cos(\theta_2) + \Pi_4 GmC_{(y,t)}\,cos(\theta_2)\right\} - \frac{w_{(y,0)}}{\Gamma(1-\alpha)}t^{-\alpha} \quad (13) $$

$$ {}^{C}\mathfrak{D}_t^{\alpha}\,T_{(y,t)} = \beta t^{\beta-1}\left\{\frac{1}{\Pi_5\,Pr}\frac{\partial^2 T_{(y,t)}}{\partial y^2}\right\} - \frac{T_{(y,0)}}{\Gamma(1-\alpha)}t^{-\alpha} \quad (14) $$

$$ {}^{C}\mathfrak{D}_t^{\alpha}\,C_{(y,t)} = \beta t^{\beta-1}\left\{\frac{1}{Sc}\frac{\partial^2 C_{(y,t)}}{\partial y^2}\right\} - \frac{C_{(y,0)}}{\Gamma(1-\alpha)}t^{-\alpha} \quad (15) $$

5. Solution of the problem

5.1. Solution of temperature field

Employing the Laplace transformation on Eq. (14) from the fractional model with its corresponding conditions, we yield

$$ q^{\alpha}\overline{T}_{(y,q)} - \overline{T}_{(y,0)} = \beta\,\Gamma(\beta)\,q^{-\beta}\left\{\frac{1}{\Pi_5\,Pr}\frac{\partial^2\overline{T}_{(y,q)}}{\partial y^2}\right\} - \frac{\overline{T}_{(y,0)}}{\Gamma(1-\alpha)}q^{-\alpha}\Gamma(1-\alpha) \quad (16) $$

With

$$ \overline{T}_{(0,q)} = \frac{1-e^{-q}}{q^2},\ \overline{T}_{(y,q)} \to 0 \quad as \quad y\to\infty $$

By utilizing the above conditions, the thermal field will become as

$$ \overline{T}_{(y,q)} = \frac{1-e^{-q}}{q^2}e^{-y\sqrt{\frac{\Pi_5\,Pr\,q^{\alpha_1}}{\beta_1}}} \quad (17) $$

To solve the Laplace inverse of Eq. (16) in Tables 3 and 4, we will employ numerical techniques such as Stehfest and Tzou's approaches.

5.2. Solution of concentration field

For the concentration field, like the thermal field, applying Laplace transformation on Eq. (15)

$$ q^{\alpha}\overline{C}_{(y,q)} - \overline{C}_{(y,0)} = \beta\,\Gamma(\beta)\,q^{-\beta}\left\{\frac{1}{\mathrm{Sc}}\frac{\partial^2\overline{C}_{(y,q)}}{\partial y^2}\right\} - \frac{\overline{C}_{(y,0)}}{\Gamma(1-\alpha)}q^{-\alpha}\Gamma(1-\alpha) \quad (18) $$

With

Table 3
Stehfest and Tzou's technique numerical analysis of temperature and velocity profile.

y	$T_{(y,t)}$ by Stehfest	$T_{(y,t)}$ by Tzou's	$C_{(y,t)}$ by Stehfest	$C_{(y,t)}$ by Tzou's	$w_{(y,t)}$ by Stehfest	$w_{(y,t)}$ by Tzou's
0.1	0.9709	0.9804	0.7034	0.7134	0.4183	0.4210
0.3	0.9485	0.9581	0.3518	0.3595	0.2810	0.2842
0.5	0.9266	0.9363	0.1710	0.1758	0.1837	0.1871
0.7	0.9051	0.9149	0.0810	0.0837	0.1170	0.1201
0.9	0.8841	0.8940	0.0375	0.0389	0.0725	0.0751
1.1	0.8636	0.8735	0.0169	0.0177	0.0438	0.0459
1.3	0.8435	0.8534	0.0075	0.0078	0.0259	0.0274
1.5	0.8238	0.8338	0.0032	0.0034	0.0151	0.0162
1.7	0.8045	0.8146	0.0013	0.0014	0.0088	0.0095
1.9	0.7857	0.7957	0.0010	0.0010	0.0051	0.0056

Table 4
Numerical analysis of Nusselt, Sherwood number, and skin friction.

α	Nu	Sh	C_f
0.1	0.5717	1.1435	1.7040
0.2	0.5975	1.1950	1.6922
0.3	0.6411	1.2823	1.6733
0.4	0.7147	1.4291	1.6432
0.5	0.8345	1.6691	1.5959
0.6	1.0199	2.0398	1.5248
0.7	1.2846	2.5692	1.4244
0.8	1.6304	3.2609	1.2930
0.9	2.0450	4.0900	1.1339

$$\overline{C}_{(0,q)} = \frac{1}{q}, \overline{C}_{(y,q)} \to 0 \quad as \quad y \to \infty$$

With the help of the above conditions, the concentration of flowing hybrid nanofluid will become

$$\overline{C}_{(y,q)} = \frac{1}{q} e^{-y\sqrt{\frac{Sc\ q^{\alpha_1}}{\beta_1}}} \tag{19}$$

In Tables 3 and 4, we will apply numerical techniques, specifically Stehfest and Tzou's approaches, to find the Laplace inverse of Eq. (19).

5.3. Solution of the velocity profile

The same technique that was used to replicate the heat transfer will also be utilized to simulate the velocity field in this area. Finally, we construct a non-homogeneous differential equation using the Laplace transformation and the corresponding boundary conditions of Eq. (13).

$$q^{\alpha}\overline{w}_{(y,q)} - \overline{w}_{(y,0)} = \beta\,\Gamma(\beta)\,q^{-\beta}\left\{\Pi_1\frac{\partial^2\overline{w}_{(y,q)}}{\partial y^2} - \beta_2\overline{w}_{(y,q)} - \left(\Pi_2 Msin(\theta_1) + \frac{\Pi_1}{K}\right)\overline{w}_{(y,q)} + \Pi_3 Gr\overline{T}_{(y,q)}\ cos(\theta_2) + \Pi_4 Gm\overline{C}_{(y,q)}\ cos(\theta_2)\right\}$$
$$- \frac{\overline{w}_{(y,q)}}{\Gamma(1-\alpha)}q^{-\alpha}\Gamma(1-\alpha) \tag{20}$$

With

$$\overline{w}_{(0,q)} = \frac{q}{q^2+\omega^2} \text{ and } \overline{w}_{(y,q)} \to 0 \quad as \quad y \to \infty$$

After using the conforming conditions, we get

$$\overline{w}_{(y,q)} = \frac{1}{1 + h\sqrt{\Pi_2 MSin(\theta_1) + \frac{\Pi_1}{K} + \beta_2 + \frac{\Pi_1\ q^{\alpha_1}}{\beta_1}}}\left[\frac{\Pi_3\ Gr(1-e^{-q})Cos(\theta_2)}{q^2}\frac{1 + h\sqrt{\frac{\Pi_5\ Pr\ q^{\alpha_1}}{\beta_1}}}{\frac{\Pi_5\ Pr\ q^{\alpha_1}}{\beta_1} - \left(\Pi_2 MSin(\theta_1) + \frac{\Pi_1}{K} + \beta_2 + \frac{\Pi_1\ q^{\alpha_1}}{\beta_1}\right)}\right.$$
$$\left. + \frac{\Pi_4\ GmCos(\theta_2)}{q^2}\frac{1 + h\sqrt{\frac{Sc\ q^{\alpha_1}}{\beta_1}}}{\frac{Sc\ q^{\alpha_1}}{\beta_1} - \left(\Pi_2 MSin(\theta_1) + \frac{\Pi_1}{K} + \beta_2 + \frac{\Pi_1\ q^{\alpha_1}}{\beta_1}\right)} + \frac{q}{q^2+\omega^2}\right] e^{-y\sqrt{\left(\Pi_2 MSin(\theta_1) + \frac{\Pi_1}{K} + \beta_2 + \frac{\Pi_1\ q^{\alpha_1}}{\beta_1}\right)}}$$
$$- \frac{\Pi_3\ Gr(1-e^{-q})Cos(\theta_2)}{q^2}\frac{e^{-y\sqrt{\frac{\Pi_5\ Pr\ q^{\alpha_1}}{\beta_1}}}}{\frac{\Pi_5\ Pr\ q^{\alpha_1}}{\beta_1} - \left(\Pi_2 MSin(\theta_1) + \frac{\Pi_1}{K} + \beta_2 + \frac{\Pi_1\ q^{\alpha_1}}{\beta_1}\right)}$$
$$- \frac{\Pi_4\ GmCos(\theta_2)}{q^2}\frac{e^{-y\sqrt{\frac{Sc\ q^{\alpha_1}}{\beta_1}}}}{\frac{Sc\ q^{\alpha_1}}{\beta_1} - \left(\Pi_2 MSin(\theta_1) + \frac{\Pi_1}{K} + \beta_2 + \frac{\Pi_1\ q^{\alpha_1}}{\beta_1}\right)} \tag{21}$$

We have used the Stehfest method, a numerical tool, to look at the thermal and momentum field solutions to investigate LT's inverse. The Gaver Stehfest algorithm [33–35] can be distinguished as follows mathematically

$$w(\xi,\tau) = \frac{ln(2)}{\tau}\sum_{n=1}^{N} v_n \overline{w}\left(\xi, n\frac{ln(2)}{\tau}\right)$$

where N is a positive integer.

$$v_n = (-1)^{n+\frac{N}{2}} \sum_{s=\left[\frac{q+1}{2}\right]}^{\min\left(p,\frac{N}{2}\right)} \frac{s^{\frac{N}{2}}(2s)!}{\left(\frac{N}{2}-s\right)!s!\,(s-1)!\,(p-s)!\,(2s-p)!}$$

We also compared and validated the results obtained by the earlier method using Tzou's methodology [36], a numerical method that may be mathematically rigorous.

$$w(\xi,t) = \frac{e^{4.7}}{t}\left[\frac{1}{2}\overline{w}\left(r,\frac{4.7}{t}\right) + Re\left\{\sum_{j=1}^{N}(-1)^k \overline{w}\left(r,\frac{4.7+k\pi i}{t}\right)\right\}\right]$$

5.4. Gradients

This article employs the Nusselt number, Sherwood number, and shear stress as the three significant main engineering numbers of significance. These gradients are stated numerically as:

$$Nu = -\left.\frac{\partial T_{(y,t)}}{\partial y}\right|_{y=0} = -\mathscr{L}^{-1}\left\{\frac{\partial \overline{T}_{(0,q)}}{\partial y}\right\}$$

$$Sh = -\left.\frac{\partial C_{(y,t)}}{\partial y}\right|_{y=0} = -\mathscr{L}^{-1}\left\{\frac{\partial \overline{C}_{(0,q)}}{\partial y}\right\}$$

$$C_f = -\left.\frac{\partial w_{(y,t)}}{\partial y}\right|_{y=0} = -\mathscr{L}^{-1}\left\{\frac{\partial \overline{w}_{(0,q)}}{\partial y}\right\}$$

6. Discussion of results

The Fractal fractional derivative, an effective and current fractional method, is used in this work to analyze the Brinkman-type hybrid-nanofluid. With water H_2O and CMC serving as the primary fluid, the suspension of hybrid nanofluids consists of graphene oxide GO and MoS_2 nanoparticles. Consideration is also given to the physical effects of an angled applied magnetic field under slip and sinusoidal heat conditions. The erect infinite inclined plate is subjected to xy-plane with porosity effect. The Prandtl number, slip

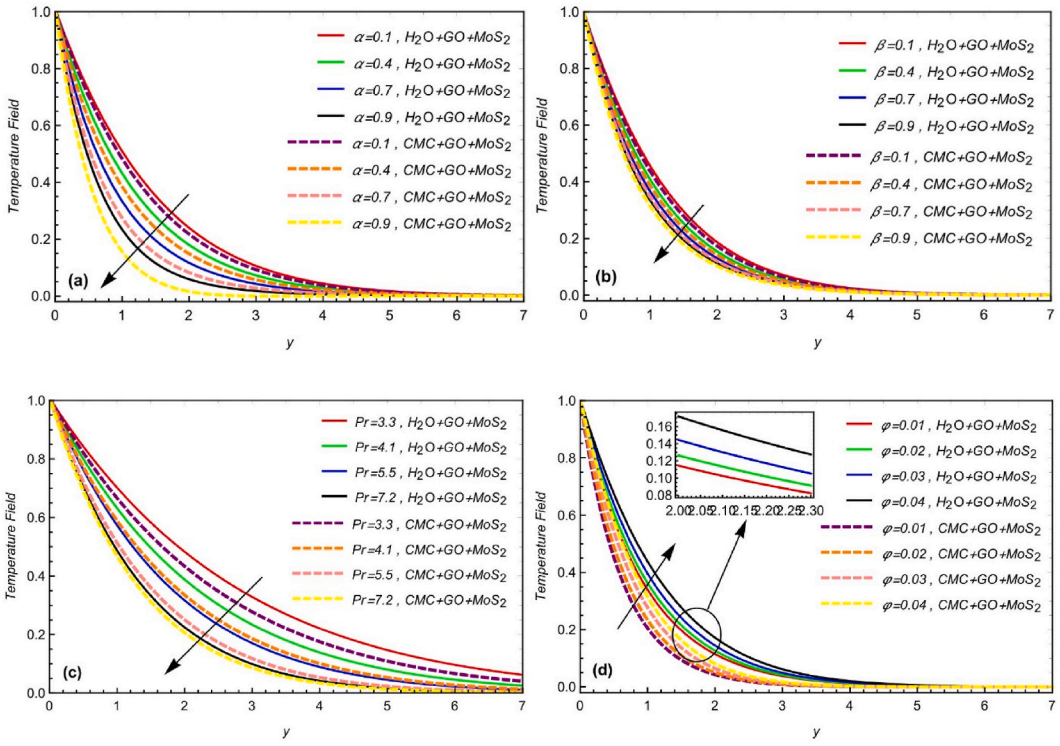

Fig. 2. Impact of **a):** α **b):** β **c):** Pr **d):** φ on the thermal profile.

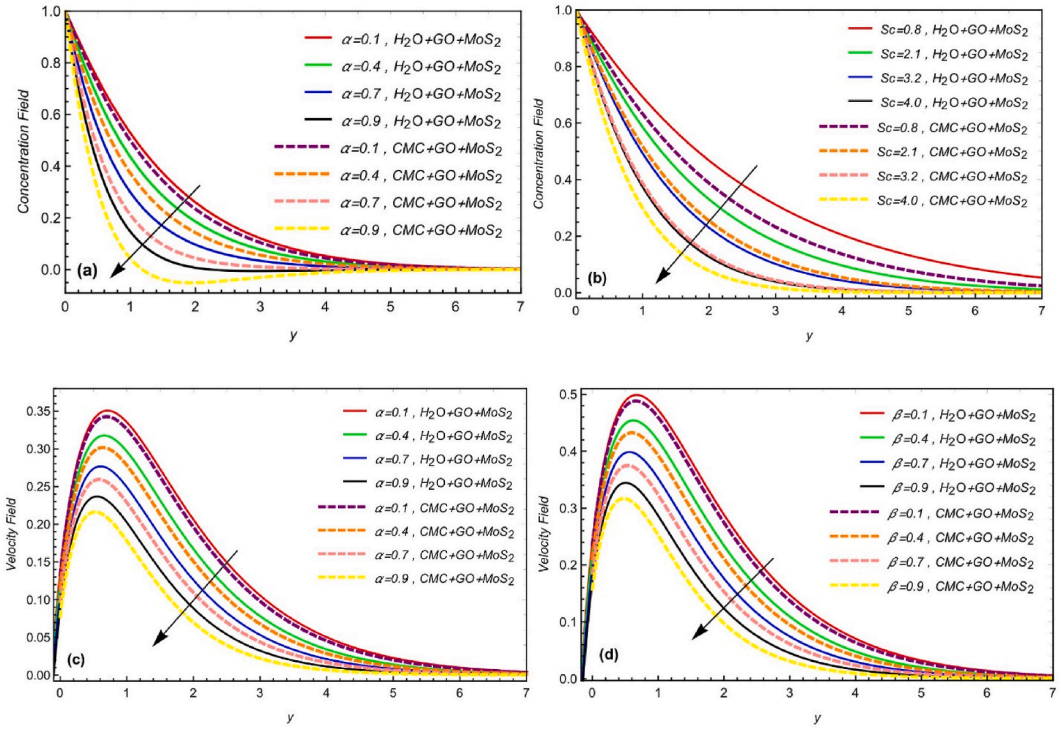

Fig. 3. Impact of fractional constraints and Schmidt number on concentration and momentum field with $\alpha = \beta = 0.7, Pr = 7.2, Sc = 3.4, \beta_2 = 1.5, Gr = 5.7, Gm = 4.3, h = 0.5, K = 1.6, M = 2.7, \varphi = 0.02, t = 0.8$.

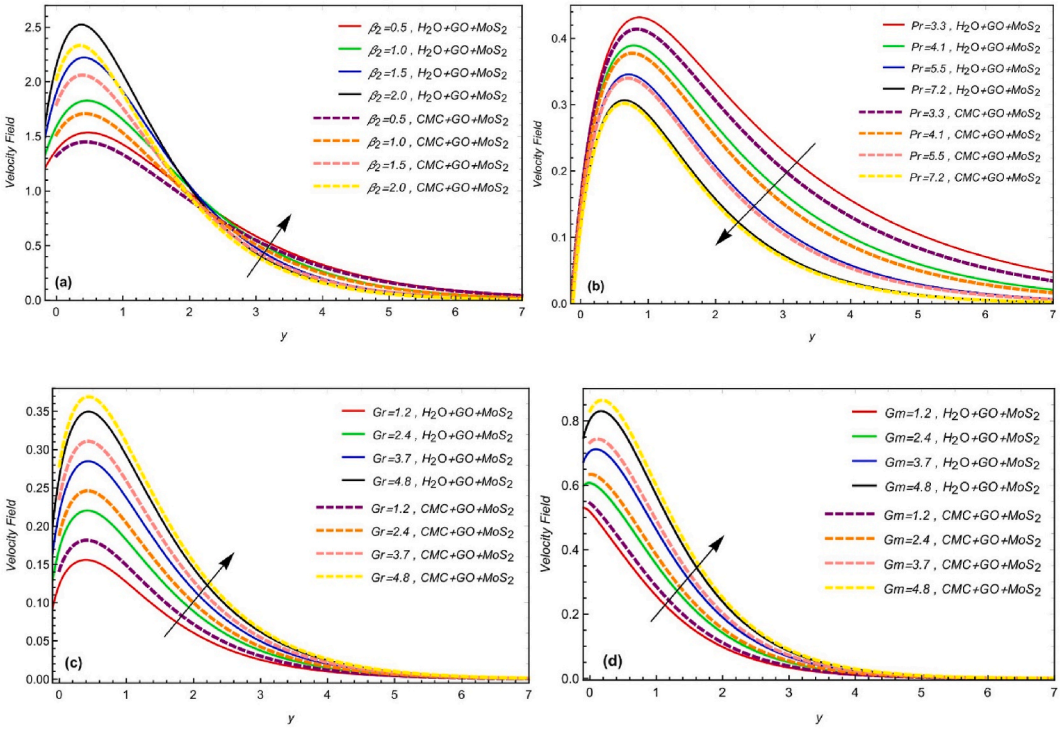

Fig. 4. Impact of **a):** β_2 **b):** *Pr* **c):** *Gr* **d):** *Gm* on momentum field with $\alpha = \beta = 0.7, Sc = 3.4, h = 0.5, K = 1.6, M = 2.7, \varphi = 0.02, t = 0.8$.

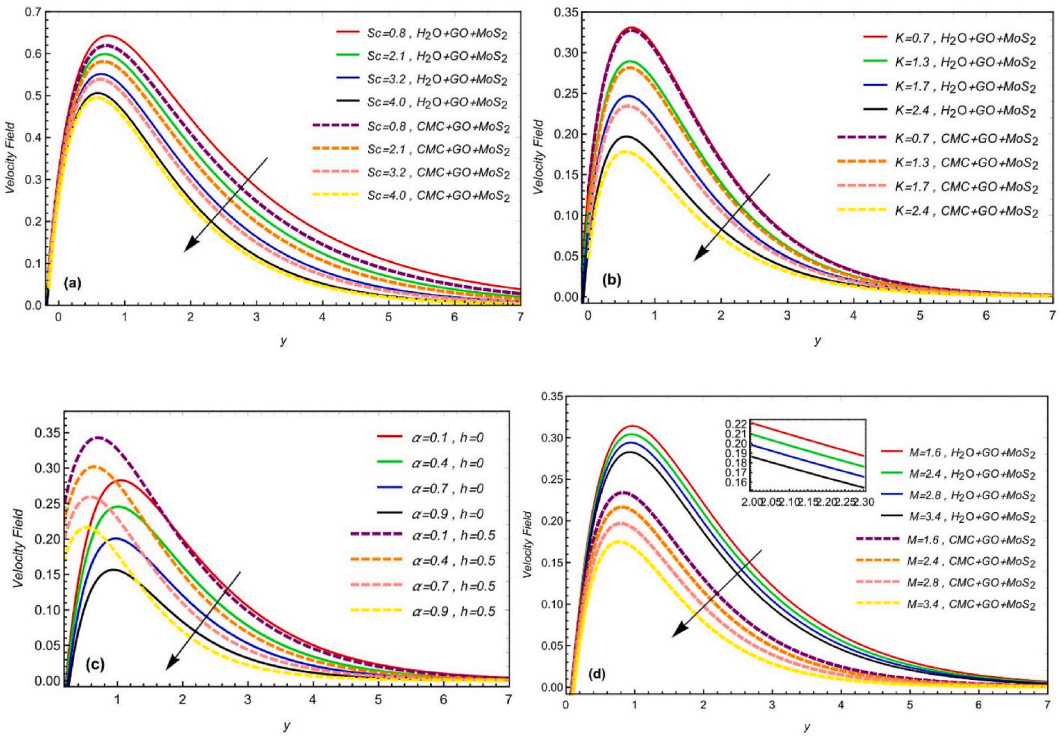

Fig. 5. Impact of **a):** Sc **b):** K **c):** h **d):** M on momentum field with $\alpha = \beta = 0.7, Pr = 7.2, \beta_2 = 1.5, Gr = 5.7, Gm = 4.3, \varphi = 0.02, t = 0.8$.

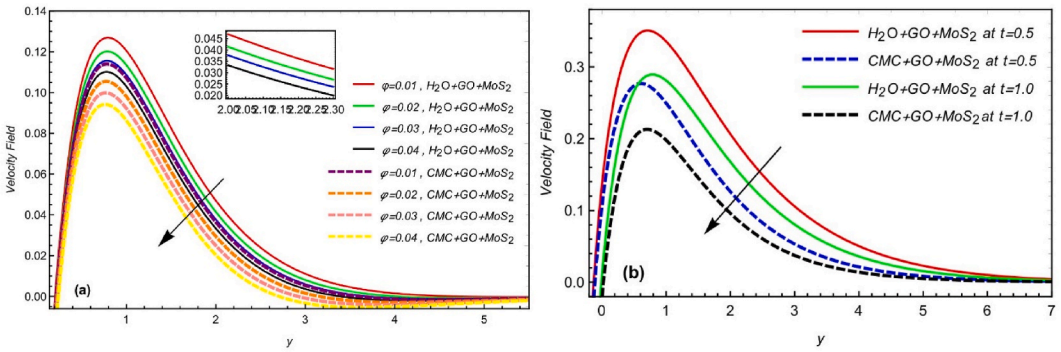

Fig. 6. Impact of **a):** φ **b):** comparison of nanofluids on momentum field with $\alpha = \beta = 0.7, Pr = 7.2, Sc = 3.4, \beta_2 = 1.5, Gr = 5.7, Gm = 4.3, h = 0.5, K = 1.6, M = 2.7, t = 0.8$.

parameter, Grashof number, and volume fraction effects of changing parameters are summarized and shown for the temperature and velocity fields from Figs. 2–7.

Holding all other constraints constant, the physical impact of fractional limitations α, β, is plotted for the temperature profile in Fig. 2(a, b). By changing the magnitudes of the fractional limitations, it can be seen that the thermal field declines exponentially. The boundary layer physically causes a drop in temperature and speed. A fractional technique is frequently preferred for regulating boundary layer thickness in fluid dynamics. Furthermore, in the comparison of considered hybrid-nanofluid, the suspension of water-based hybrid-nanofluid $(H_2O + GO + MoS_2)$ has a more significant impact on the thermal field as compared to carboxymethyl cellulose-based hybrid-nanofluid $(H_2O + GO + MoS_2)$ due to the physical characteristics of considered nanoparticles and base fluid. Fig. 2(c, d) compares the effective Prandtl number Pr and volume fraction φ to y while all other constraints are constant. In terms of graphics, it has reached the stage where liquid temperature decreases as the Prandtl number Pr rises, while the thermal field grows when volume fraction values increase. Raising Pr shortens the thermic conduction as expected since the thickness of the boundary layer is reduced by the high viscosity. In addition, physically, the fluid becomes hotter by improving its thermal conductivity by adding more nanoparticles to the base fluid. The temperature profile increases with the increment in volume fraction constraint. The influence of the fractional value on the fluid's concentration regime is depicted in Fig. 3(a, b) for different nanoparticles. The related boundary layer

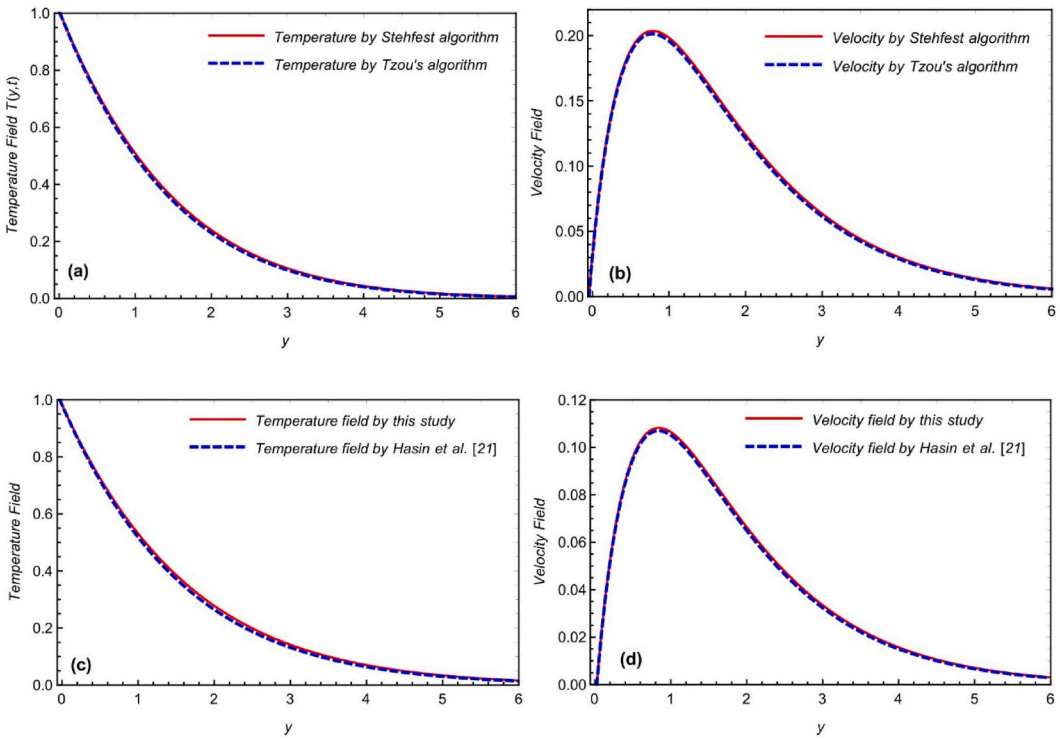

Fig. 7. Comparison of numerical schemes and with the results of Hasin et al. [21].

thickness of the concentration field is increased by fixing other factors as constants and increasing the value of *Sc*. The impact of *Sc* on the concentration domain is depicted in Fig 3(b). It has been noted that when *Sc* increases, the fluent's density reduces, which impacts the rate of molecular diffusion and tends to minimize boundary layer thickness.

The flow velocity is displayed for a range of values for α, β, by holding the other parameters constant. It was evident that the fractional order differential operator, in contrast to the integer order differential operator, is nonlocal since the system's later stages depend on both the current scene and its prior stages. Given that it has a better kernel that preserves memory information and is better at representing the flow fields of fluids, it performs a better job of explaining the behavior of the fractional constraints. The visual record makes it clear that velocity falls as α, β value increases. In other words, the speed of a fluid flow can be controlled by fractional limits. Viscous forces are strengthened by a rise in α, β as opposed to thermal forces, which tend to slow down fluid velocity. Again like the thermal profile in the comparison of considered hybrid-nanofluid, the water-based hybrid-nanofluid $(H_2O + GO + MoS_2)$ has a bit more significant impact on momentum profile as compared to carboxymethyl cellulose-based hybrid-nanofluid $(H_2O + GO + MoS_2)$ due to the physical characteristics of considered nanoparticles and base fluid.

Fig. 4(a) displays the effects of the Brinkman factor on the velocity profile. Velocity depicts the dual behavior for Brinkman-type parameters. Initially, speed increases for β_2 but then this alternates its behavior, and the fluid moves more slowly with the enhancement of β_2. The cause is because increasing values of the Brinkman parameter result in stronger drag forces and decreasing velocity. Fig. 4(b) depicts *Pr* impact on momentum. It was evident that when *Pr* increases, the fluid velocity falls and that the thickness of the stratum boundary is likely to decrease as well because *Pr* raises the viciousness and causes the thermic stratum boundary to move more slowly. The momentum field used to examine the impact of *Gr* and *Gr* is illustrated in Fig. 4(c, d). With increasing the value of the grashof number, a rise in velocity profile has been seen. Physically, the increase in heat and mass grashof number from more generated fluid flows is caused by a rise in buoyancy effects. As a result, these forces may affect increasing velocity.

The impact of Schmidt number *Sc* for the momentum field is depicted in Fig 5(a). Again velocity field decreases with the enhancement in *Sc* parameter. The influence of *K* on the velocity distribution for both types of hybrid nanofluids is shown in Fig. 5(b). It has been observed that higher values of K. reduce the velocity field. This results in a decrease in the thickness of the momentum boundary layer due to a reduction of the resistance of the porous material. In Fig. 5(c, d), the effects of the slip parameter and applied magnetic field can be analyzed. The manipulation of the magnetic number M is covered in Fig. 5(d). The velocity must decrease for the magnetic values obtained to increase. The Lorentz force is significantly influenced by the electromagnetic force, which opposes the fluid's velocity. Physically, at large values of M, this is true because M intensifies the Lorentz forces, which tend to slow velocity. The effects of the φ_{hnf} volume fraction on hybrid nanoparticles and comparison of different hybrid nanofluids are depicted in Fig. 6(a, b). It is determined that the temperature can rise for a higher φ_{hnf} values and velocity-indicated dips. The velocity field is significantly influenced favorably by the nanofluid density. When base fluid and nanoparticles are combined, the resulting hybrid nanofluids dramatically thicken, which slows velocity and raises temperature. Furthermore, the speed of water-based suspension of hybrid

nanofluids ($H_2O+GO+MoS_2$) is a bit more as compared to the suspension of carboxymethyl cellulose-based hybrid nanofluid ($CMC+GO+MoS_2$) due to the physical characteristics of considered nanoparticles and base fluids.

Ultimately, we compared our findings with those of Hasin et al. [21] for different numerical schemes. It is evident that the justification for the overlap of all curves for momentum and thermal profile validity and the validation of our obtained results may be made. Furthermore, compared to the exponential kernel and generalized Mittage-Leffler present in CF and AB-fractional derivative, the solution obtained with generalized Fractal fractional kernel exhibits stronger memory. The conclusion states that our results are more improved in terms of memory. Tables 3 and 4 use several methods to analyze the controlled model's numerical output. The numerical validation of achieved results using different numerical systems is shown in Table 3. The Sherwood number and Nusslt number values for skin friction are shown in Table 4 as well.

7. Conclusions

In this paper, an unsteady, viscous, and incompressible Brinkman-type hybrid nanofluid mixed with graphene oxide (GO) and molybdenum disulfide (MoS_2) with the suspension of water (H_2O) and carboxymethyl cellulose (CMC) as base fluids are discussed. A practical and modern fractional derivative approach, specifically the Fractal fractional derivative and LT scheme, is used to solve an under problem. Several inverse techniques, such as Stehfest and Tzou's algorithms, are used to numerically show and compare the effects of various constraints with modified values for the heat and velocity fields. The following statements sum up the main results of the graphical representation:

- The heat transfer drops by raising the quantities of fractional restrictions and Prandtl number.
- By altering the fractional restraint values, the velocity gradient slows down while accelerating when the Grashof number is increased.
- As a comparison to different hybrid nanofluids, the velocity field has a somewhat higher value for water (H_2O) based suspension as compared to carboxymethyl cellulose (CMC).
- The solution using fractal fractional derivative presents excellent comparison findings with current simulations.
- Validity and justification of obtained results can be gained by overlapping curves in comparing numerical techniques and with the results of Hasin et al. [21].

Author statement

Ali Raza: Conceptualization, Methodology, Original draft preparation, Data curation.
Rifaqat Ali: Conceptualization, Methodology, Writing- Original draft preparation.
Sayed M. Eldin: Methodology, Investigation, Resources, Writing- Reviewing and Editing.
Suleman H. Alfalqui: Investigation, Resources. Original draft preparation, Ali Hasan Ali: Software, Visualisation, Supervision, Writing- Reviewing and Editing.

Declaration of competing interest

The authors declare that they have no known competing financial interests or personal relationships that could have appeared to influence the work reported in this paper.

Data availability

Data will be made available on request.

Acknowledgment

The authors thank the Deanship of Scientific Research at King Khalid University for funding this work through a large group research project under Grant number RGP 2/86/44.

References

[1] S. Akram, S. Nadeem, Influence of induced magnetic field and heat transfer on the peristaltic motion of a Jeffrey fluid in an asymmetric channel: closed form solutions, J. Magn. Magn Mater. 328 (2013) 11–20.
[2] M. Boujelbene, S. Rehman, S. Alqahtani, S. Alshehery, S.M. Eldin, Thermal transport and magnetohydrodynamics flow of generalized Newtonian nanofluid with inherent irreversibility between conduit with slip at the walls, Eng. Appl. Comput. Fluid Mech. 17 (2023), 2182364.
[3] M.M. Bhatti, S. Mishra, T. Abbas, M.M. Rashidi, A mathematical model of MHD nanofluid flow having gyrotactic microorganisms with thermal radiation and chemical reaction effects, Neural Comput. Appl. 30 (2018) 1237–1249.
[4] A. Hajizadeh, N.A. Shah, S.I.A. Shah, I. Animasaun, M. Rahimi-Gorji, I.M. Alarifi, Free convection flow of nanofluids between two vertical plates with damped thermal flux, J. Mol. Liq. 289 (2019), 110964.
[5] A.H. Seikh, A. Akinshilo, M. Taheri, M. Rahimi-Gorji, N. Alharthi, I. Khan, et al., Influence of the nanoparticles and uniform magnetic field on the slip blood flows in arterial vessels, Phys. Scripta 94 (2019), 125218.
[6] W. Ibrahim, G. Kuma, Magnetohydrodynamic flow of a nanofluid due to a non-linearly curved stretching surface with high order slip flow, Heat Tran. Asian Res. 48 (2019) 3724–3748.
[7] A.U. Khan, S. Hussain, S. Nadeem, Existence and stability of heat and fluid flow in the presence of nanoparticles along a curved surface by mean of dual nature solution, Appl. Math. Comput. 353 (2019) 66–81.
[8] S. Nadeem, M.R. Khan, A.U. Khan, MHD stagnation point flow of viscous nanofluid over a curved surface, Phys. Scripta 94 (2019), 115207.

[9] M. Gholinia, M. Armin, A. Ranjbar, D. Ganji, Numerical thermal study on CNTs/C2H6O2–H2O hybrid base nanofluid upon a porous stretching cylinder under impact of magnetic source, Case Stud. Therm. Eng. 14 (2019), 100490.
[10] B. Souayeh, K.G. Kumar, M.G. Reddy, S. Rani, N. Hdhiri, H. Alfannakh, et al., Slip flow and radiative heat transfer behavior of Titanium alloy and ferromagnetic nanoparticles along with suspension of dusty fluid, J. Mol. Liq. 290 (2019), 111223.
[11] I. Waini, A. Ishak, I. Pop, Flow and heat transfer along a permeable stretching/shrinking curved surface in a hybrid nanofluid, Phys. Scripta 94 (2019), 105219.
[12] S. Nadeem, N. Abbas, M. Malik, Inspection of hybrid based nanofluid flow over a curved surface, Comput. Methods Progr. Biomed. 189 (2020), 105193.
[13] N. Jabeen, N.U. Hassan, A. Bokhari, M.F. Khan, S.M. Eldin, W.U. Arifeen, et al., High performance δ-Bi2O3 nanosheets transformed Bi2S3 nanoflakes interconnected nanosheets as negative electrode for supercapacitor applications, Fuel 347 (2023), 128392.
[14] R. Abdelhak, F. Redouane, W. Jamshed, M.R. Eid, K. Guedri, M.I.U. Rehman, et al., Analysis of water conveying aluminum oxide/silver nanoparticles due to mixed convection through four square cavity's variable hot (cold) walled, Ain Shams Eng. J. 14 (2023), 102072.
[15] K. Zheng, A. Raza, A.M. Abed, H. Khursheed, L.F. Seddek, A.H. Ali, A.U. Haq, New fractional approach for the simulation of (Ag) and (TiO2) mixed hybrid nanofluid flowing through a channel: fractal fractional derivative, Case Stud. Therm. Eng. 45 (2023), 102948.
[16] M.S. Khan, M.A. Memon, I. Khan, S.M. Eldin, Finite element based direct and iterative approach to investigate a magneto-micropolar flow through a rectangular channel, Alex. Eng. J. 75 (2023) 55–66.
[17] S. Nadeem, B. Ishtiaq, J. Alzabut, S.M. Eldin, Three parametric Prabhakar fractional derivative-based thermal analysis of Brinkman hybrid nanofluid flow over exponentially heated plate, Case Stud. Therm. Eng. 47 (2023), 103077.
[18] K. Zhang, N.A. Shah, M. Alshehri, S. Alkarni, A. Wakif, S.M. Eldin, Water thermal enhancement in a porous medium via a suspension of hybrid nanoparticles: MHD mixed convective Falkner's-Skan flow case study, Case Stud. Therm. Eng. 47 (2023), 103062.
[19] Y. Masthanaiah, N. Tarakaramu, M.I. Khan, A. RushiKesava, S.B. Moussa, B.M. Fadhl, et al., Impact of viscous dissipation and entropy generation on cold liquid via channel with porous medium by analytical analysis, Case Stud. Therm. Eng. 47 (2023), 103059.
[20] S.K. Rawat, M. Yaseen, U. Khan, M. Kumar, A. Abdulrahman, S.M. Eldin, et al., Insight into the significance of nanoparticle aggregation and non-uniform heat source/sink on titania–ethylene glycol nanofluid flow over a wedge, Arab. J. Chem. 16 (2023), 104809.
[21] F. Hasin, Z. Ahmad, F. Ali, N. Khan, I. Khan, A time fractional model of Brinkman-type nanofluid with ramped wall temperature and concentration, Adv. Mech. Eng. 14 (2022), 16878132221096012.
[22] D. Khan, G. Ali, A. Khan, I. Khan, Y.-M. Chu, K.S. Nisar, A new idea of fractal-fractional derivative with power law kernel for free convection heat transfer in a channel flow between two static upright parallel plates, Comput. Mater. Continua (CMC) 65 (2020) 1237–1251.
[23] A. Raza, N. Nigar, U. Khan, S. Elattar, S.M. Eldin, A.M. Abed, Comparative investigation of fractional bioconvection and magnetohydrodynamic flow induced by hybrid nanofluids through a channel, Front. Mater. 10 (2023), 1143612.
[24] A. Raza, M.Y. Almusawa, Q. Ali, A.U. Haq, K. Al-Khaled, I.E. Sarris, Solution of water and sodium alginate-based casson type hybrid nanofluid with slip and sinusoidal heat conditions: a prabhakar fractional derivative approach, Symmetry 14 (2022) 2658.
[25] A. Raza, A.U. Haq, S. Farid, A Prabhakar fractional approach with generalized fourier law for thermal activity of non-Newtonian second-grade type fluid flow: a fractional approach, Waves Random Complex Media (2022) 1–17.
[26] S. Rana, R. Tabassum, R. Mehmood, E.M. Tag-eldin, R. Shah, Influence of Hall current & Lorentz force with nonlinear thermal radiation in an inclined slip flow of couple stress fluid over a Riga plate, Ain Shams Eng. J. (2023), 102319.
[27] M. Ahmad, M.I. Asjad, K.S. Nisar, I. Khan, Mechanical and thermal energies transport flow of a second grade fluid with novel fractional derivative, Proc. IME E J. Process Mech. Eng. (2021), 09544089211053561.
[28] A. Atangana, Fractal-fractional differentiation and integration: connecting fractal calculus and fractional calculus to predict complex system, Chaos, Solit. Fractals 102 (2017) 396–406.
[29] A. Atangana, M.A. Khan, Validity of fractal derivative to capturing chaotic attractors, Chaos, Solit. Fractals 126 (2019) 50–59.
[30] M. Imran, Application of fractal fractional derivative of power law kernel (FFP0Dxα, β) to MHD viscous fluid flow between two plates, Chaos, Solit. Fractals 134 (2020), 109691.
[31] N.A. Sheikh, F. Ali, M. Saqib, I. Khan, S.A.A. Jan, A.S. Alshomrani, et al., Comparison and analysis of the Atangana–Baleanu and Caputo–Fabrizio fractional derivatives for generalized Casson fluid model with heat generation and chemical reaction, Results Phys. 7 (2017) 789–800.
[32] M. Imran, F. Miraj, I. Khan, I. Tlili, MHD fractional Jeffrey's fluid flow in the presence of thermo diffusion, thermal radiation effects with first order chemical reaction and uniform heat flux, Results Phys. 10 (2018) 10–17.
[33] A. Raza, A.M. Abed, M. Almusawa, L.F. Seddek, A.H. Ali, Prabhakar fractional simulation for inspection of CMC-based nanofluid flowing through a poured vertical channel, Case Stud. Therm. Eng. (2023), 102911.
[34] M.I. Khan, I.B. Mansir, A. Raza, S.U. Khan, S. Elattar, H.M. Said, et al., Fractional simulations for thermal flow of hybrid nanofluid with aluminum oxide and titanium oxide nanoparticles with water and blood base fluids, Nanotechnol. Rev. 11 (2022) 2757–2767.
[35] S. Ullah Khan, A. Raza, B. Prasannakumara, Y.D. Reddy, M.I. Khan, Inspecting heat transport phenomenon in the flow of non-Newtonian fluid in the presence of Newtonian heating and inclined slip: fractional derivative framework, Waves Random Complex Media (2023) 1–12.
[36] A. Raza, U. Khan, Z. Raizah, S.M. Eldin, A.M. Alotaibi, S. Elattar, et al., Numerical and computational analysis of magnetohydrodynamics over an inclined plate induced by nanofluid with Newtonian heating via fractional approach, Symmetry 14 (2022) 2412.